Capillary Condensation in a Geometrically and a Chemically Heterogeneous Pore: A Molecular Simulation Study

Joël Puibasset[†]

Centre de Recherche sur la Matière Divisée, CNRS-Université d'Orléans, 1b, rue de la Ferollerie, 45071 Orléans Cedex 02, France

Received: December 3, 2003; In Final Form: August 26, 2004

A computer simulation study has been carried out, using an extended Gibbs ensemble Monte Carlo technique, to examine the influence of so-called geometric and chemical disorder on the thermodynamic behavior of simple fluids confined in porous media. The technique allows the equilibrium coexistence of gas and liquid phases to be calculated in a single run. The phase diagram of Lennard-Jones fluid has been calculated in a perfectly cylindrical pore as a reference. Some disorder is then introduced in the porous material, first by spatially modifying the external potential of the initially cylindrical pore, to imitate the geometric disorder of a more realistic pore (undulation, constrictions, etc.) and second by modulating the amplitude of the same initially cylindrical potential to reproduce the energetic disorder of realistic pores due to chemical variations along it. It is shown that the chemical disorder has a much stronger effect on the phase diagram of the confined fluid. The complete adsorption/desorption isotherms are also calculated to help in understanding the large effects of chemical disorder.

Introduction

The effect of confinement on phase behavior of simple fluids is still an area of intensive research. Between experiment and theory, molecular simulation is a powerful tool to study the confinement effect in realistic porous materials, because it allows for the introduction of some degree of disorder in the substrate model. Most of previous simulation studies,[1−5] which aimed at establishing the phase diagram of a confined Lennard-Jones-like fluid, were restricted to simple pore geometries (slits or cylinders). The development of the Gibbs ensemble Monte Carlo technique by Panagiotopoulos[2,6,7] greatly favored the study of such simple systems. The technique is very efficient to calculate the phase diagram, because each run (at a given temperature) converges directly to the equilibrium state (if it exists) between a gaslike and a liquidlike phase. However, due to the volume exchange procedure between the two phases, at least one invariant direction of space is required for applicability of this method, which is the case essentially (but not exclusively) for slits or cylinders. Generally, the introduction of some disorder in such simple pores breaks the initial translation invariance in one of the space directions and prevents it from working in the Gibbs ensemble. The molecular simulation techniques for such disordered systems are numerous [grand canonical Monte Carlo (GCMC), molecular dynamics, NPT + test particle method, histogram reweighting, gauge cell method, etc.],[8−14] but all require the calculation of full isotherms and a lengthy integration procedure to calculate the free energy which gives the equilibrium and finally the phase diagram.[15−21] The case of a symmetric Lennard-Jones mixture in a disordered solid matrix[22] has been treated in the Gibbs ensemble thanks to symmetry considerations, as well as the case of a disordered porous solid in the limit of very low density (few percent).[23,24]

In this work, we focus on two weakly disordered pores, for which the Gibbs ensemble Monte Carlo technique can still be applied. One of the pores is geometrically undulated, whereas the second is cylindrical but presents a chemical variation which gives rise to a modulation of the wall potential. In the first case, almost no change in the phase diagram is observed, whereas in the second, strong modifications are reported. The adsorption−desorption isotherms are also calculated. They show also the strong influence of chemical disorder compared to that of geometrical disorder.

Pore Geometries, Interaction Model, and Computational Details

The aim of this work is to establish the phase diagram of fluids adsorbed in slightly disordered porous substrates. The system represents fluid argon in various porous CO_2 solids. The pores are approximately 2.7 nm in diameter, and they are supposed to be rigid and structureless. This smooth wall approximation consists of integrating locally the fluid wall interaction, which minimizes the memory required to save the external potential felt by the fluid, and accelerating the calculations during the course of the simulation. Nevertheless, the size of the pore is thought to be large enough compared to the smoothing length (few interatomic distances) so as to catch the physics of the adsorption phenomena. The peculiar choice of argon adsorbed in solid CO_2 pores has been motivated by the fact that this system has already been chosen to study phase diagrams of fluids confined in cylindrical pores.[1−3,25,26] This makes this work a natural continuation of previous studies and allows for fruitful comparison between ordered (previous work)[2,3] and disordered pores (this work). The advantage of this system is that the depth of the interatomic potential is relatively low, which involves strong modifications of the phase diagram due to confinement.

The Lennard-Jones (6,12) potential

$$u_{ij}(r_{ij}) = 4\epsilon_{ij}[(\sigma_{ij}/r_{ij})^{12} - (\sigma_{ij}/r_{ij})^{6}] \qquad (1)$$

is used to model all interactions in the system. No distance cutoff

[†] E-mail: puibasset@cnrs-orleans.fr.

10.1021/jp037696d CCC: $30.25
Published on Web 02/12/2005

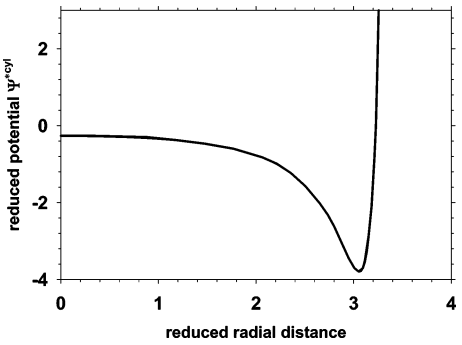

Figure 1. Reduced potential ψ^{cyl} inside the perfectly cylindrical pore versus the reduced radial distance.

is used, and minimal image convention is applied.[9] We did not perform long-range corrections either, because they cannot be easily calculated for inhomogeneous phases as in cylinders. Furthermore, Panagiotopoulos has shown that this correction would have minimal influence on the calculations.[2] The parameters describing fluid−fluid and fluid−solid interactions are given in Table 1 and correspond to those used in previous works.[2,3,26] The fluid−fluid parameters are those chosen to normalize all thermodynamic quantities. The density of the solid is taken to be equal to 1530 kg/m^3, which gives a reduced particle density $\rho_{solid}^* = \rho_{solid}\sigma_{f-f}^3 = 0.8265$.

TABLE 1: Argon/Solid CO_2 Interaction Parameters

	ϵ/k_B (K)	σ (Å)
fluid−fluid (f−f)	119.8	3.405
wall−fluid (w−f)	153.0	3.725

The reference pore is a cylinder of 2.724 nm in diameter, which corresponds to a reduced diameter of 8. The potential inside the cylindrical pore is calculated by considering that the wall sites are distributed uniformly inside the wall. With such a prescription the external potential has a cylindrical symmetry and can be expressed as a function of the radial distance only. The reduced potential $\psi^{*cyl} = \psi^{cyl}/\epsilon_{f-f}$ is shown in Figure 1, versus the reduced radial distance.

The thermodynamic properties of the fluid confined in this cylindrical pore have been calculated as a reference. The pore has then been modified in two different ways: the first one mimics geometric disorder, while the second one mimics chemical disorder. In both cases the potential is now dependent on the axial direction z, by introducing some sinusoidal undulation in the position (geometric disorder) or in amplitude (chemical disorder), as follows:

$$\psi^{*geo}(r, z) = \psi^{*cyl}\left(r/\left\{1 - a\cos\left(\frac{2\pi z}{L}\right)\right\}\right) \quad (2)$$

$$\psi^{*chem}(r, z) = \left\{1 + a\cos\left(\frac{2\pi z}{L}\right)\right\}\psi^{*cyl}(r) \quad (3)$$

where $\psi^{*geo}(r, z)$ [respectively $\psi^{*chem}(r, z)$] is the reduced potential in the geometrically (respectively chemically) disordered pores, $\psi^{*cyl}(r)$ is the potential in the perfectly cylindrical pore (see Figure 1), a is a measure of the amplitude of the heterogeneity, taken equal to 0.25 in this work, and L is the length of the simulation box, equal to $12\sigma_{f-f}$. The radius of the geometrically undulated pore varies between $3\sigma_{f-f}$ for $z = 0$ and $5\sigma_{f-f}$ for $z = \pm L/2$. In this system, the disorder consists of an enlargement of the pore size distribution up to 25% of its average value. For the second system the pore radius is constant, but the intensity of the fluid/wall interaction varies within 25% of its average value: this mimics some chemical disorder with more attractive sites and less attractive sites distributed along the pore.

The geometric undulation produces a potential which is not very realistic because it deforms the potential well in the narrowest region of the pore. However, the aim of this study was to produce a geometrically deformed pore which has exactly the same volume distribution of external potential as the perfectly cylindrical one. In other words, a unique particle moving in the pore has to experience statistically exactly the same external potential in both the cylindrical and the geometrically deformed pore. The geometric deformation of eq 2 naturally satisfies such a requirement.

The state of the fluid in the pores is described by the adsorbed quantity or coverage equal to the number of particles in the simulation box divided by the reduced volume $V^* = V/\sigma_{f-f}^3$

$$\Gamma^* = \frac{1}{V^*}\int_{-L/2}^{+L/2}\int_0^R r\rho(r, z)\,dr\,dz \quad (4)$$

The quantity V is defined as the volume of space where the potential is not infinite. In the case of the cylindrical pore of reduced radius 4, the volume is $V^{cyl} = 16\pi L\sigma_{f-f}^2$. The volume of the chemically heterogeneous pore is exactly the same because both potentials are infinite in the same region of space: $V^{chem} = 16\pi L\sigma_{f-f}^2$. The volume of the undulated pore is calculated by integration of the sinusoidal modulation: $V^{geo} = 16.5\pi L\sigma_{f-f}^2$. It is larger than the cylindrical volume.

The calculations are made in an extension of the Gibbs ensemble Monte Carlo method[2,6] which allows the pressure and the chemical potential of two different phases to be equilibrated in a single run. The simulation ensemble is made of two independent boxes, each containing one of the two coexisting phases adsorbed in the pore. Random displacements are performed in each box to ensure thermal equilibrium. The maximal amplitude of the displacement is modulated to ensure a 50% acceptance ratio. Every 10 displacement trials in each box, it was decided to perform particle interchange to ensure chemical equilibrium and volume change to ensure mechanical equilibrium. The maximal amplitude for the volume exchange is adjusted to give an acceptance ratio equal on the average to 50%. The volume exchange consists of varying, on one hand, the volume of one of the simulation boxes, containing the first phase and, on the other hand, the volume of the second simulation box so as to keep the total volume constant. In systems presenting a translation invariance, like perfectly cylindrical cylinders, Panagiotopoulos[2] has proposed performing volume variations by changing the size of the simulation box in the axial direction of the pore. However, in pores presenting heterogeneities in the axial direction it is impossible to expand the size of the simulation box in this direction without changing the intrinsic geometrical characteristics of the pores (curvature, pore size distribution, surface heterogeneities, etc.). This is why we use instead the rotational invariance. This idea is derived from a thermodynamic formalism similar to the classical one which can be developed by using rotational invariance, in the same spirit as the spherical invariance is used in the case of a droplet.[27] See also the work of Nishioka[28,29] for a recent application of this thermodynamic formalism to surface tension calculations of spherical interfaces. To better illustrate the procedure of interest, let us focus on the two-dimensional case, where the system would be a disk containing adsorbed two-dimensional molecules (the edge of the disk would be the substrate; see Figure 2a). The position of each particle is identified by its radial coordinate r and its angular coordinate

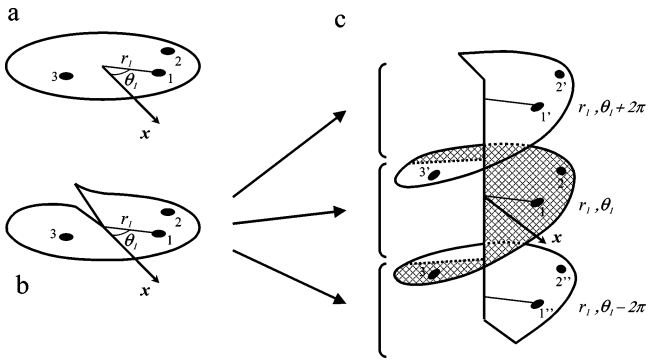

Figure 2. (a) Two-dimensional disklike pore showing three particles and the cylindrical coordinates for particle 1. (b) Same system after a radial cut along the radius opposite to the angular reference axis *x*. (c) Stacking of identical systems as in part b, showing the first 2π periodic images of each particle; the "dilatation" along the helix axis is for clarity of the figure.

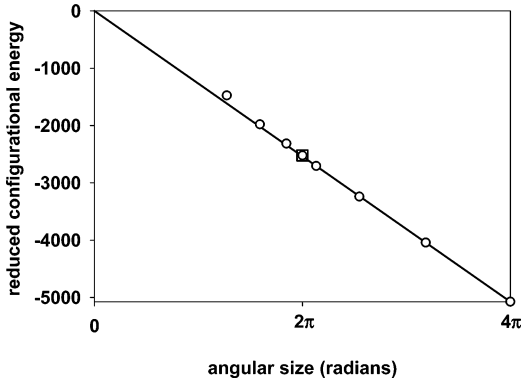

Figure 3. Circles: reduced configurational energy of the helix representation of the system as a function of the angular size (or period of the helix), in the canonical ensemble. Square: same quantity for the original system.

θ defined from a given reference axis *x*. Let us cut the disk along a radius (for instance chosen at $\theta = \pi$), raise one of the edges, and lower the other one to form the beginning of a helix (Figure 2b). An infinite helix can then be constructed by simply repeating this initial portion of the helix, the final result being the periodic helix of Figure 2c, which shows the periodic images (1′, 1″, etc.) of the initial particles. Note that the images of a given particle at radial distance *r* from the center and angular coordinate θ from a given origin (in cylindrical coordinates) are at the same radial distance *r* from the center and angular coordinates $\theta + 2k\pi$ where *k* is an integer. Let us now focus on the interactions between these particles: if one considers that two particles can interact only if the absolute difference between their angular coordinates is less than π, then each molecule sees exactly one image of each of the other molecules (minimal image convention). Then, the configurational energy (and actually all thermodynamic properties) of the infinite periodic system per period is exactly the configurational energy of the original system (which is 2π periodic). This helix (exact) representation can be easily generalized to the three-dimensional case, the helix being now a four-dimensional object. The application of the periodic boundary conditions in the third direction (along the axial coordinate in the three-dimensional undulated pore) follows the usual procedure: a particle moving out of the box through one side is re-injected through the opposite side at the same radial and angular coordinates. We have now an infinitely periodic and exact representation of our system which enables continuous volume variations. These volume variations are carried out simply by applying an expansion to the angular coordinates, or in other words, we simply change the period of the helix which is now not necessarily equal to 2π rad any more. The successive replicas of a molecule are then not aligned any more parallel to the helix axis. Of course, the minimal image convention is still applied in the same spirit so that each molecule will still experience the same forces as if the system was not made helix-periodic. If the period is exactly 2π, then the system can be easily represented on the paper (which is 2π periodic). If the period is exactly 4π, it can also be represented on the paper by two systems equivalent to the original one (the volume has then been multiplied by 2, without changing any geometric characteristics such as the radius of the pore), and so forth. The strength of the helix representation is that it actually allows any period to be considered, not necessarily an integral multiple of 2π, which cannot be easily represented in our geometric space. However, in all cases it can always be locally represented because the helix is locally flat everywhere from a topological point of view. The local flatness is actually required: the space has to be flat on any extension corresponding to the range of the interactions (short-range Lennard-Jones-like in our case) so that the local structure of the fluid or the spatial pair correlation function $g(r)$ is not distorted by the topology of the helix.

The last point to be checked is that the extensive thermodynamic quantities are actually proportional to the length of the period of the helix (at constant density) or, in other words, proportional to the size of the system. We illustrate this point by considering the configurational energy of a Lennard-Jones fluid confined in a cylindrical pore. The external potential produced by the pore is described in the next section. The number of particles is chosen to keep the density at the constant value of 0.52 in reduced units, which corresponds to a dense phase. The temperature is fixed, and the total energy is allowed to fluctuate in the canonical ensemble. The average value of the configurational energy is reported in Figure 3 (circles) as a function of the length of the period of the helix (size of the system) in radians. As can be seen, the energy is essentially proportional to the size of the system except for values of the period significantly lower than 2π which certainly introduces over-correlations in the system. The square corresponds to the same quantity calculated in the original pore, without using the helix representation. The value coincides exactly with that obtained in the helix representation. This exact correspondence and the proportionality of the configurational energy with the period of the helix for values not necessarily multiple of 2π meets exactly the requirement for such extensive thermodynamic quantities. The period of the helix is, thus, a good parameter to modulate continuously the size of the system while keeping all geometric and physicochemical characteristics constant (pore size distribution, chemical heterogeneities, etc.). We have then an exact representation of the original system which enables continuous variations of volume without distorting any intrinsic geometric parameter of the porous system. Such continuous variations allow the implementation of the Gibbs ensemble Monte Carlo method.[6] The new method has been checked in the special case of the perfectly cylindrical pore, where both this new extended and the conventional[2] techniques can be applied. The phase diagrams are identical, which validates the technique.

Influence of Geometric and Chemical Disorder on Phase Diagrams of Confined Fluids

The confined fluid phase diagram is obtained by reporting the reduced densities of the coexisting phases as a function of

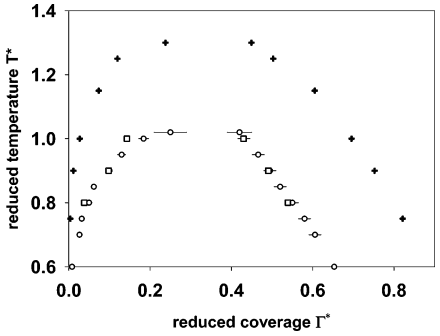

Figure 4. Phase diagram of Lennard-Jones fluid confined in perfectly cylindrical pore (circles, this work; squares, ref 2). The crosses correspond to the bulk phase diagram (from refs 2 and 6).

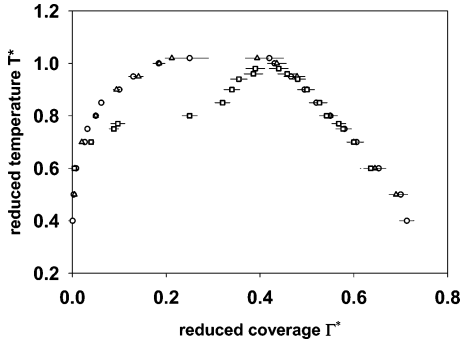

Figure 5. Phase diagram of the Lennard-Jones fluid confined in perfectly cylindrical pore (circles), geometrically undulated pore (triangles), and chemically undulated pore (squares).

the reduced temperature $T^* = k_B T/\epsilon_{f-f}$, where k_B is Boltzman's constant. The first calculations were performed in the cylindrical pore, that is to say by using the potential $\psi^{*cyl}(r)$ previously defined. Thus, the results can be directly compared to phase diagrams previously obtained by other authors. The results for the cylindrical pore correspond to the circles shown in Figure 3. For comparison, independent results found in the literature[2] for the same system are deferred in the form of squares on Figure 4. As can be seen the agreement is quite good, especially in the liquid phase. This last point shows that our calculation of the pore volume (in this work, it is defined as the volume where the potential is not infinite, as in ref 2) is consistent with previous work, because the liquid density in the pore is very sensitive to the definition of the empty volume of the pore. On the other hand, while in agreement, the points in the gas phase show some discrepancies, essentially at high temperature. However, inspection shows that the three reported points from literature present an upward curvature, whereas a downward curvature is expected. The uncertainty on these points is then probably a bit larger, and all results are certainly compatible. This agreement validates our implementation of the extended Gibbs ensemble method in cylindrical geometries. The bulk Lennard-Jones coexistence curve from refs 2 and 6 is also reported. As a general comment, one can see that confinement strongly affects the thermodynamics of the adsorbed fluid. Essentially, the gas phase is denser, probably due to the external potential which traps some molecules. We shall come back to this point while discussing the adsorption isotherms. On the other hand the liquid phase has a lower density, due partly to the depletion (hard core repulsion) very close to the wall. Note that this decrease of the liquid density is also partly due to the definition of the empty volume. However, the lowering of the critical temperature is independent of such definitions and corresponds physically to the disappearance of phase coexistence. In the confined geometry, the critical temperature is 1.05, versus 1.3 in bulk.

The second calculation, for the geometrically undulated pore, is performed by simply changing the external potential from $\psi^{*cyl}(r)$ to $\psi^{*geo}(r, z)$ and changing the total volume to V^{geo} in the normalization of the amount of adsorbed fluid. The results for the undulated pore are shown as triangles in Figure 5, as well as those of the perfectly cylindrical pore (circles) for comparison. As can be seen, the phase diagrams are surprisingly identical. Panagiotopoulos has shown the influence of the pore diameter on the shape of the phase diagram.[2] He has shown that the coexistence curve for pores of radius $3\sigma_{f-f}$ is significantly displaced to lower values, with a reduced critical point around 0.95. On the other hand, for pores of radius $5\sigma_{f-f}$, the phase diagram is closer to the bulk limit, with a critical point a bit lower than 1.1. It is surprising that for the undulated pore considered in this paper, which presents a lowest radius of $3\sigma_{f-f}$ and a largest radius of $5\sigma_{f-f}$ the coexistence curve seem to follow an intermediate path between the coexistence lines of pores of radius $3\sigma_{f-f}$ and $5\sigma_{f-f}$, that is to say very close to the coexistence line of the pore of radius $4\sigma_{f-f}$. This discussion will be completed later, when the adsorption isotherms are calculated.

The third calculation concerns the chemically disordered pore. The external potential is switched to $\psi^{*chem}(r, z)$ and the normalization volume to V^{chem}. The results are shown in Figure 5 (squares). As can be seen, the phase diagram for the chemically disordered pore is strongly distorted compared to the perfectly cylindrical pore. For very low temperature, the differences between coexistence curves are not so evident. Concerning the liquid phase, because it has a very low compressibility the density is not much affected by a 25% increase of the external potential in some region of the pore and a 25% decrease in other regions. On the other hand, the effect on the gas density cannot be clearly seen on this diagram due to its low value. This point will be re-discussed later on the basis of adsorption isotherms. Nevertheless, above a reduced temperature of 0.7, the density of the saturated gaslike phase starts to become much higher in the chemically disordered pore, probably due to large adsorption in the most attractive regions of the pore. On the other hand, the density of the liquidlike phase is not affected by the external potential up to higher temperature, which explains the unusual shape of the coexistence line. As a matter of fact the critical temperature in the heterogeneous pore is relatively close to the one in the homogeneous pore, whereas the critical density is significantly displaced to higher values. This has already been observed on lattice systems by Pitard and co-workers[30] and in molecular systems by Reszko-Zygmunt and co-workers.[19]

Adsorption Isotherms in Geometrically and Chemically Disordered Pores

To get more insight on the reason the phase diagram is more influenced by the chemical disorder than the geometric disorder, we have calculated both the adsorption and desorption isotherms in the different pores. The numerical method used in this calculation is the GCMC algorithm.[8] The volume of the simulation box, the temperature, and the chemical potential are kept constant during the simulation: therefore, it mimics a real adsorption experiment where volume and temperature are controlled and the chemical potential is fixed through the pressure of the gas reservoir. From a technical point of view, the simulation consists, on one hand, in thermal equilibration of the simulation box through molecular displacements with acceptance probabilities determined by the ratio of the difference in energy to the external temperature and, on the other hand, in

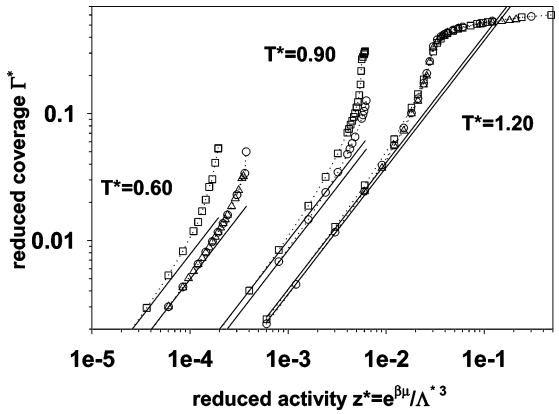

Figure 6. Adsorption branches at three different temperatures for the perfectly cylindrical pore (circles), the geometrically undulated pore (triangles), and the chemically undulated pore (squares). The solid lines correspond to the perfect gas approximation calculated from the space integral (see Table 2).

chemical equilibration with a particle reservoir through addition or removal of particles in the simulation box with probabilities determined by the imposed chemical potential. For a complete and detailed explanation of the technique, see ref 8. Note that, in a real adsorption experiment, the adsorbate is introduced progressively to be adsorbed in the previously outgassed porous sample. Similarly, the initial molecular configuration is an empty pore, used as the starting point of the simulation at very low pressure. The pressure of the gas reservoir is then increased by steps to calculate the whole adsorption isotherm. For each step, the initial configuration is the final configuration of the preceding step. At least 10^5 Monte Carlo trials per molecule are performed to reach equilibrium, and then at least twice as many are performed to acquire statistics. When the saturation of the sample is reached, one can start to calculate the reverse path by decreasing the pressure. The obtained so-called desorption branch is generally not identical to the adsorption branch (hysteresis). The adsorption and desorption isotherms have been calculated in the geometrically undulated and the perfectly cylindrical pore at two reduced temperatures, 0.60 and 1.20, and in the chemically heterogeneous and the perfectly cylindrical pore at three reduced temperatures, 0.60, 0.90, and 1.20. This choice corresponds to one supercritical temperature and one or two subcritical temperatures of special interest (see phase diagrams Figure 5). The isotherms are presented as a function of reduced activity $z^* = e^{\mu^*/T^*}/\Lambda^{*3}$. This choice is motivated by the fact that this quantity is probably more intuitive than chemical potential and more directly comparable to experiments. Furthermore, the adsorbed amount is related to the activity independently of the value attributed to the mass of the particle, which is not the case for the chemical potential. The adsorption branches are shown in Figure 6 in logarithmic scale to enlarge low densities. They are compared to their perfect-gas approximation, calculated in the external potential created by the porous solid according to the formula

$$\rho^* = \frac{e^{\mu^*/T^*}}{\Lambda^{*3}} \frac{1}{V^*}\int d\mathbf{r}^*\, e^{-\Psi_{ext}^*/T^*} = z^* \frac{1}{V^*}\int d\mathbf{r}^*\, e^{-\Psi_{ext}^*/T^*} \quad (5)$$

obtained by integrating the "barometric law",[27] where ρ^* is the reduced density of the perfect gas, μ^* the reduced chemical potential, Λ^* is the reduced de Broglie's wavelength, and the integral of the exponential of the external potential ψ_{ext}^* is performed over the accessible reduced volume V^*. The values obtained as a numeric calculation of the space integral in eq 5 (normalized to the volume) for the cylindrical and the geometrically and chemically disordered pores are given in Table 2. As can be seen, the space integral in the undulated pore is exactly the same as in the perfectly cylindrical one. This is due to the fact that the undulation is created by a simple geometric deformation of the cylindrical potential. It can then be concluded that these pores are energetically exactly identical. They only differ from a topological point of view. This point justifies the construction of this pore by simply deforming the initially cylindrical potential instead of recalculating the real potential in an undulated pore: the energetics is kept constant in the first case, whereas the second construction, although more realistic, would introduce both geometric and energetic disorder. Figure 6 shows that all GCMC adsorption branches converge to their respective perfect gas approximation at low density. Let us now focus on the comparison of the results for the geometrically disordered and the perfectly cylindrical pore. For a given temperature, the isotherms look very similar, showing the weak influence of the geometrical disorder. This is expected because the topology cannot influence the low density part of the adsorption isotherm. In other words, the isolated molecules adsorbed at low pressure cannot feel the geometrical disorder at a given instant because they are punctual. This would not be the case for dynamical quantities like the diffusion process because in this case one would look at spatial or temporal correlations. Let us now focus on the effect of the chemical disorder and compare the GCMC simulation results for the adsorption isotherms in the chemically disordered pore and the cylindrical pore for the three reduced temperatures: 0.60, 0.90, and 1.20 (see Figure 6). In this case the branches are not identical, even at the supercritical temperature of 1.20 where close inspection shows disagreement at low pressure. For every temperature, the low pressure adsorption branches are different. This difference is directly related to the values of the space integrals given in Table 2. The 25% modulation of the external potential creates some regions of space where the potential is lower, which contributes to the integral. As a consequence, the complete integration gives a value which is 50% higher at the temperature of 0.60. Furthermore, the higher the temperature the lower the difference. This explains the fact that the low pressure differences in adsorption branches are less pronounced at higher temperature. Moreover, one can see that at low temperature the effect of the chemical disorder becomes stronger when the chemical potential is increased, whereas at high temperature the influence of chemical disorder disappears when the chemical potential increases. At the supercritical temperature, $k_B T = 1/\beta$, which appears in the Monte Carlo probability ratio, becomes larger than the difference in energy between the different configurations of molecules in the pore. As a consequence, the whole pore can be explored by the molecules. In other words, the kinetic energy is high enough for the particles to explore the whole pore. They are less sensitive to the external potential and then to the 25% chemical disorder. On the other hand, at low temperature ($T^* = 0.60$), particles concentrate in regions of low external potential, which results in an increased coverage. This increase actually triggers the fluid condensation

TABLE 2: Normalized Space Integral $1/V^* \int d\mathbf{r}^*\, e^{-\Psi_{ext}^*/T^*}$ for the Perfectly Cylindrical and the Geometrically and Chemically Disordered Pores for Different Temperatures

T^*	perfect cylinder	geometrically disordered	chemically disordered
0.60	49.5	49.5	77.5
0.90	8.35	8.35	10.0
1.20	3.77	3.77	4.11

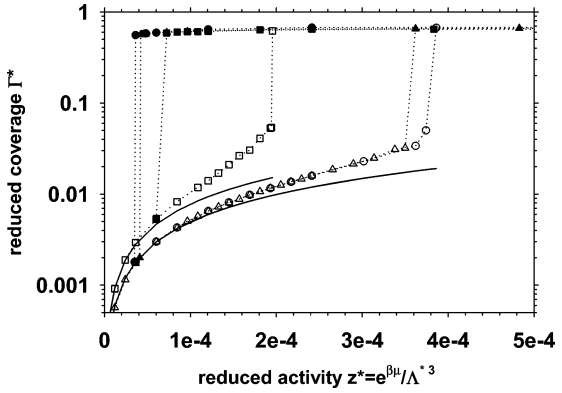

Figure 7. Complete adsorption (empty symbols)/desorption (filled symbols) isotherms at $T^* = 0.60$ for the perfectly cylindrical pore (circles), the geometrically undulated pore (triangles), and the chemically undulated pore (squares). The solid lines correspond to the perfect gas approximation. Dotted lines are guides to the eyes.

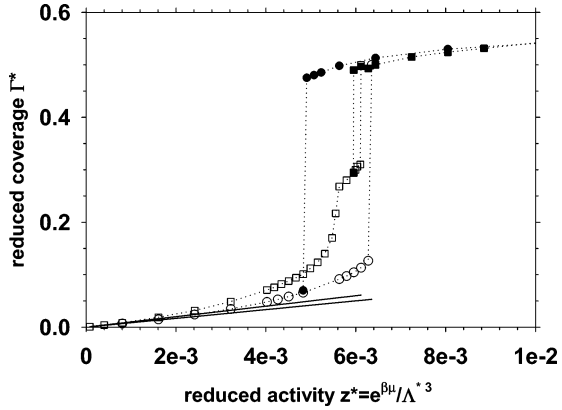

Figure 8. Complete adsorption (empty symbols)/desorption (filled symbols) isotherms at $T^* = 0.90$ for the perfectly cylindrical pore (circles) and the chemically undulated pore (squares). The solid lines correspond to the perfect gas approximation. Dotted lines are guides to the eyes.

(end of the gas branch) at significantly lower activity or chemical potential ($z^* = 1.93 \times 10^{-4}$) compared to the perfect cylinder case ($z^* = 3.66 \times 10^{-4}$). It is interesting to note that both adsorption branches end when the same value of the coverage is reached: $\Gamma^* = 0.050$ for the perfect cylinder and $\Gamma^* = 0.054$ for the chemically disordered pore. It is proposed that this correlation is a direct consequence of the fact that both pores are geometrically identical. It seems that the gas instability which controls the "capillary condensation" jump is essentially controlled by geometric considerations. The chemical disorder simply displaces the jump to lower chemical potential. On the other hand, the comparison of the adsorption branches for the cylindrical and the undulated pore shows that the geometrical disorder has almost no influence on the value of the coverage at a given pressure, except that the gas instability happens at a lower density in the geometrically disordered pore ($\Gamma^* = 0.032$) and consequently at a lower pressure and chemical potential ($z^* = 3.50 \times 10^{-4}$) compared to the perfect cylinder ($\Gamma^* = 0.050$, $z^* = 3.66 \times 10^{-4}$). This comparison shows that, despite the fact that both pores are energetically equivalent (superimposable adsorption branches), the geometrical disorder displaces the gas instability to lower chemical potential by destabilization of lower coverage configurations. It is proposed that the nucleation of the liquidlike phase, the origin of the instability, is favored by the geometric disorder, more precisely in the narrowed portions of the pore. Such a mechanism has already been observed by Coasne and Pellenq.[31]

In the case of the chemically disordered pore, the phase diagram is strongly distorted around $T^* = 0.90$ (see Figure 5). This feature is also visible in the adsorption isotherm (see Figure 6). The coverage in the chemically disordered pore rapidly increases just above the gas instability point due to enhanced condensation of gas in the pore. Contrary to the preceding case, the gas instability points are not characterized by identical coverage. In this case, the adsorbed phases are probably not comparable, and the chemical disorder seems able to favor a denser phase, probably due to regions of lower potential. However, this denser phase is less stable with respect to the capillary condensation because the gas instability point in the chemically disordered pore is displaced to lower chemical potential compared to that of the perfectly cylindrical pore.

Figures 7 and 8 show the complete adsorption−desorption isotherms at the reduced temperatures of 0.60 and 0.9. The logarithmic scale is used in Figure 7 to enlarge the very low density gas branches. The high (supercritical) temperature (1.20) isotherms are reversible: the desorption branches are identical to the adsorption ones of Figure 6 and, therefore, not represented. On the other hand, the low temperature isotherms present a hysteresis. In all cases the loop is limited by the adsorption and desorption branches and two vertical lines of various length. In no case do the adsorption or desorption branches meet at some point. At fixed temperature, there is no continuous path joining the gaslike and liquidlike branches, which allows one to consider them as two distinct "phases". Figures 7 and 8 show that, as a general trend, the higher the temperature, the smaller the hysteresis loop, which actually disappears in the vicinity of the critical temperature. Figures 7 and 8 show that all liquid branches are superimposable: the geometrical and chemical disorder does not affect much the dense phase. This explains why the position of the saturating liquid branch of the phase diagram is not affected by disorder. At low temperature ($T^* = 0.60$) the liquid instability point (left vertical line) is not influenced by geometric disorder but is displaced to higher pressure by chemical disorder. This last point is also visible at $T^* = 0.90$ (Figure 8). It is proposed that the local density of the fluid is not much affected by geometric variations but is strongly affected by chemical disorder. In the less attractive regions of the pore, the fluid density is probably lower, which acts as a nucleation center of the gas phase. A density profile study is underway to clarify these questions.

Conclusion

More and more molecular simulation studies on fluid adsorption in porous solids direct toward realistic pores presenting some degree of disorder. In this work, simple examples of disorder have been considered. This disorder has been produced by modulating the external potential of an initially perfectly cylindrical pore. The geometric disorder is reproduced by a spatial deformation of the potential, and the energetic or chemical disorder is mimicked by a modulation of the amplitude of the external potential. The phase diagrams of the fluid adsorbed in the two disordered pores have been calculated in the framework of the modified Gibbs ensemble Monte Carlo method, and the adsorption isotherms have been determined in the grand canonical ensemble. The main conclusion that can be drawn after this study is that the geometrical disorder has almost no influence on the thermodynamics of the confined fluid, whereas the chemical disorder strongly modifies its adsorption properties. More precisely, the geometric disorder slightly shortens the gas adsorption branch by destabilizing the adsorbed gas at high pressure, without modifying the amount

of adsorbed gas. On the other hand, the chemical disorder induces a strong increase of the adsorbed amount, especially just below the critical point, which shortens the gas adsorption branch, but also displaces the saturated gas branch of the phase diagram to higher densities. The rest of the phase diagram is essentially the same as for the perfectly cylindrical pore. It is to be noted that despite the strong displacement of the saturating gas branch of the phase diagram toward the saturating liquid branch, the critical temperature is not much affected. However, the critical density is increased.

Acknowledgment. It is a pleasure to thank A. Delville, R. J.-M. Pellenq, and B. Coasne for very interesting discussions on the Gibbs ensemble technique and pore constrictions. P. Porion is also gratefully acknowledged for very stimulating questions throughout this work. The simulations were performed locally on workstations purchased thanks to grants from Région Centre (France).

References and Notes

(1) Heffelfinger, G. S.; van Swol, F.; Gubbins, K. E. *Mol. Phys.* **1987**, *61*, 1381.
(2) Panagiotopoulos, A. Z. *Mol. Phys.* **1987**, *62*, 701.
(3) Peterson, B. K.; Gubbins, K. E. *Mol. Phys.* **1987**, *62*, 215.
(4) Vishnyakov, A.; Piotrovskaya, E. M.; Brodskaya, E. N. *Langmuir* **2001**, *17*, 4451.
(5) Peterson, B. K.; Gubbins, K. E.; Heffelfinger, G. S.; et al. *J. Chem. Phys.* **1988**, *88*, 6487.
(6) Panagiotopoulos, A. Z. *Mol. Phys.* **1987**, *61*, 813.
(7) Smit, B.; DeSmedt, P.; Frenkel, D. *Mol. Phys.* **1989**, *68*, 931.
(8) Nicholson, D.; Parsonage, N. G. *Computer simulation and the statistical mechanics of adsorption*; Academic Press: London, 1982.
(9) Allen, M. P.; Tildesley, D. J. *Computer simulation of liquids*; Clarendon Press: Oxford, 1987.
(10) Panagiotopoulos, A. Z. *J. Phys.: Condens. Matter* **2000**, *12*, R25.
(11) Frenkel, D.; Smit, B. *Understanding Molecular Simulation*; Academic Press: London, 1996.
(12) Neimark, A. V.; Vishnyakov, A. *Phys. Rev. E* **2000**, *62*, 4611.
(13) Möller, D.; Fischer, J. *Mol. Phys.* **1990**, *69*, 463.
(14) Möller, D.; Fischer, J. *Mol. Phys.* **1990**, *75*, 1461.
(15) Alvarez, M.; Levesque, D.; Weis, J.-J. *Phys. Rev. E* **1999**, *60*, 5495.
(16) Page, K. S.; Monson, P. A. *Phys. Rev. E* **1996**, *54*, R29.
(17) Page, K. S.; Monson, P. A. *Phys. Rev. E* **1996**, *54*, 6557.
(18) Sarkisov, L.; Monson, P. A. *Phys. Rev. E* **2000**, *61*, 7231.
(19) Reszko-Zygmunt, J.; Pizio, O.; Rzysko, W.; et al. *J. Colloid Interface Sci.* **2001**, *241*, 169.
(20) Sacquin, S.; Schoen, M.; Fuchs, A. H. *J. Chem. Phys.* **2003**, *118*, 1453.
(21) Pellenq, R. J.-M.; Levitz, P. *Mol. Phys.* **2002**, *100*, 2059.
(22) Gordon, P. A.; Glandt, E. D. *J. Chem. Phys.* **1996**, *105*, 4257.
(23) Brennan, J. K.; Dong, W. *J. Chem. Phys.* **2002**, *116*, 8948.
(24) Brennan, J. K.; Dong, W. *Phys. Rev. E* **2003**, *67*, 031503.
(25) Peterson, B. K.; Gubbins, K. E.; Heffelfinger, G. S.; et al. *J. Chem. Phys.* **1988**, *88*, 6487.
(26) Peterson, B. K.; Walton, J. P. R. B.; Gubbins, K. E. *J. Chem. Soc., Faraday Trans. II* **1986**, *82*, 1763.
(27) Rowlinson, J. S.; Widom, B. *Molecular Theory of Capillarity*; Clarendon Press: Oxford, 1982.
(28) Nishioka, K. *Phys. Rev. A* **1977**, *16*, 2143.
(29) Nishioka, K. *Phys. Rev. A* **1987**, *36*, 4845.
(30) Pitard, E.; Rosinberg, M. L.; Tarjus, G. *Mol. Simul.* **1996**, *17*, 399.
(31) Coasne, B.; Pellenq, R. J.-M. *J. Chem. Phys.* **2004**, *120*, 2913.